Simulation of Unsaturated Flow Using Richards Equation

Rowan Cockett
Department of Earth and Ocean Science
University of British Columbia
rcockett@eos.ubc.ca

Abstract

Groundwater flow in the unsaturated zone is a highly nonlinear problem that is described by Richards equation. In this work I present a finite-volume approximation of Richards equation in one-, two-, and three-dimensions. The nonlinearities in the equation can lead to changes in soil conductivity over several orders of magnitude. As such the problem is stiff, and requires a fully-implicit time discretization. A Newton root-finding algorithm is described in detail and is compared to two different Picard implementations. Several numerical examples and rigorous testing show the validity and usefulness of the Newton root-finding implementation presented.

1 Introduction & Motivation

Studying the processes that occur in the vadose zone, the region between the earth's surface and the fully saturated zone, is of critical importance for the understanding of our groundwater resources. The majority of groundwater recharge is derived through water that percolates through the vadose zone. As such, much attention has been given to monitoring and describing processes that occur in this region of the earth. Hydraulic conductivity is a property of the soil media and is the main regulator of groundwater flow. However, in many field investigations the hydraulic conductivity is often unknown or only known as a bulk average at various distinct points. As hydraulic conductivity is the main parameter of interest, an accurate estimate that is spatially consistent with the media is highly valuable. In saturated aquifers pumping-tests and slug-tests inject or extract water and measure the response of hydraulic-head, which is related to the hydraulic conductivity. The parameter estimates are a volume-average of the aquifer and the extent of the measurement varies proportionally to the volume of water injected or extracted in the test. The radial extent from a tested well can vary over several orders of magnitude from 10^{-1}m in slug tests to 10^{3}m in multi-day pumping tests. It is more complicated to estimate hydraulic conductivity in unsaturated media because the hydraulic conductivity is a function of saturation. Field tests include infiltration experiments where the goal is to saturate the soil to remove the dependence on saturation. These infiltration experiments typically do not fully saturate the soil and as such can consistently underestimate the saturated hydraulic conductivity. Laboratory experiments on core-samples are also regularly completed but are expensive, time-consuming, and average a small portion of the media that may not be representative.

The measurements and tests for hydraulic conductivity typically done in a hydrogeologic field investigation yield point-measurements that are bulk averages of the media. With only a small amount of data, groundwater models can often be over simplifications of the true process, which limits their usability. Geophysical methods can provide additional data that is spatially and temporally extensive. This data, however, is not a direct measurement of the hydrogeologic parameters of interest and must be processed in such a way that it is usable to hydrologists.

The goal of fully coupling a geophysical model and a groundwater flow model is the motivation for the current work. However, before the two models can be coupled both the geophysical model and the groundwater flow model must be constructed and carefully tested. The work presented in this paper will describe, implement, and test a groundwater flow model for use in the unsaturated vadose zone.

2 Background

2.1 Richards Equation

Flow in the vadose zone has many complications as the parameters that control the flow are dependent on the saturation of the media, leading to a non-linear problem. Flow in the vadose zone is referred to as unsaturated flow, and is described by Richards equation. The groundwater flow equation has a diffusion term, as well as an advection term that is related to gravity and only acts in the z-direction. There are two different forms of Richards equation that will be considered in this paper that differ on how they deal with the non-linearity in the time-stepping term. The most fundamental form is called the mixed form of Richards Equation [*Celia et al.*, 1990]:

$$\frac{\partial \theta(\psi)}{\partial t} - \nabla \cdot K(\psi) \nabla \psi - \frac{\partial K(\psi)}{\partial z} = 0 \tag{1}$$

where θ is water content, and ψ is pressure head. This formulation of Richards equation is called the 'mixed'-form because the equation is parameterized in ψ but the time-stepping is in terms of θ. The most commonly used formulation of Richards equation is known as the head-based form, and is popular because the time-stepping is explicitly written in terms of ψ.

$$C(\psi)\frac{\partial \psi}{\partial t} - \nabla \cdot K(\psi) \nabla \psi - \frac{\partial K(\psi)}{\partial z} = 0 \tag{2}$$

where $C(\psi) = \frac{\partial \theta}{\partial \psi}$ and is called the specific moisture capacity function. The differences in discretization and benefits in choosing between these two formulations will be discussed in detail in this paper.

An important aspect of unsaturated flow is noticing that both water content and hydraulic conductivity are functions of pressure-head (ψ). There are many empirical relations used to relate these parameters, including the Brooks-Corey model and the Van Genuchten model [*van Genuchten*, 1980]. The Van Genuchten model is slightly more popular when modeling because there are no discontinuities in the functions, unlike the Brooks-Corey model. A version of the Van Genuchten model is written [*Celia et al.*, 1990]:

$$\theta(\psi) = \frac{\alpha(\theta_s - \theta_r)}{\alpha + |\psi|^\beta} + \theta_r \tag{3a}$$

$$K(\psi) = K_s \frac{A}{A + |\psi|^\gamma} \tag{3b}$$

Where parameters α, β, γ, and A are fitting parameters that are often assumed to be constant in the media; θ_r and θ_s are the residual and saturated moisture contents; and K_s is the saturated hydraulic conductivity. An example of the curves using Van Genuchten parameters from *Celia et al.* [1990] is shown in Figure 1. Small changes in pressure head can change the hydraulic conductivity several orders of magnitude; as such, $K(\psi)$ is a highly nonlinear function. The water content curve is also highly nonlinear as saturation can change dramatically over a small range of pressure head values (Figure 1). It should be noted that these functions are only valid when the pressure-head ψ is negative; that is, the media is semi-saturated. When the media is fully saturated $K = K_s$ and θ is equal to the porosity.

Typical uses of Richards equation are to simulate infiltration experiments in both the laboratory and the field scale. These experiments begin with an initially dry soil and then add water to the top of the core sample (or ground surface). The simulation of this experiment requires simulating fast changes in pressure head and saturation over the most nonlinear part of the Van Genuchten curves. This experiment is the motivation for the discretization scheme that is described in the following section.

3 Discretization

Richards equation is parameterized in terms of pressure head (ψ) in both the mixed- and the head-based forms. This paper describes simulating Richards equation for one-, two-, and three-dimensions, however, special attention is paid to the one-dimensional case. The spatial discretization for Richards equation was chosen to be a finite-volume approximation; this is a natural extension of mass-conservation in a volume where the balance of fluxes into and out of a volume is conserved. In two-dimensions the flux into and out of a volume can be seen in Figure 2. Here it is natural to assign the entire cell one hydraulic conductivity value, which is located at the cell center. Assigning the cell-center the value for hydraulic conductivity, rather than a cell face or node, has the interpretation that a single value fills the entire

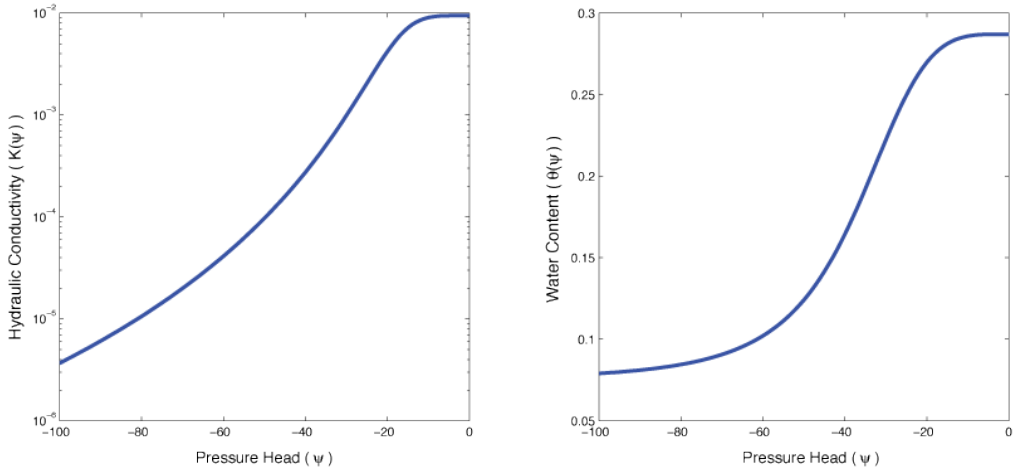

Figure 1: Example Van Genuchten curves for (a) hydraulic conductivity and (b) water content. Parameters used from Equation 3 are $\alpha = 1.611 \times 10^6$, $\theta_s = 0.287$, $\theta_r = 0.075$, $\beta = 3.96$, $A = 1.175 \times 10^6$, $\gamma = 4.74$, $K_s = 9.44 \times 10^{-5}$ m/s.

cell and allows for discontinuities between adjacent cells. From a geologic perspective discontinuities are prevalent, as you can have large differences in hydraulic properties between layers in the ground. The pressure-head data will also be located at the cell centers. The discretization chosen results in a staggered mesh in space. The details of the spatial and temporal discretization will be outlined in the following two sections.

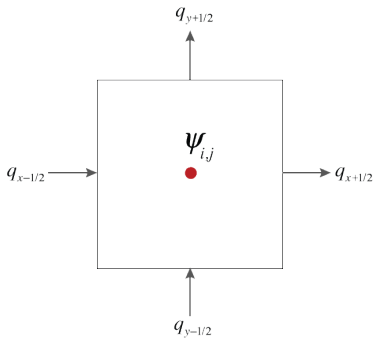

Figure 2: Finite volume grid in 2D showing flux into and out of a single cell.

3.1 Spatial Discretization

Richards equation is discretized on a cell-centered finite volume mesh, and the discrete approximation will be explicitly written for one-dimension. Ignoring the discretization of the time derivative, Richards equation can be written in matrix form:

$$\frac{\partial \theta(\psi)}{\partial t} - \mathbf{D}\,\text{diag}\left(\frac{1}{\mathbf{A}_v \frac{1}{K(\psi^{n+1})}}\right)\mathbf{G}\psi - \mathbf{D}_z\left(\frac{1}{\mathbf{A}_v \frac{1}{K(\psi^{n+1})}}\right) = 0 \tag{4}$$

Here $\mathbf{D}$ and $\mathbf{G}$ are the discretized divergence and gradient operators, respectively. The derivative in the z-direction is written $\mathbf{D}_z$, and in one-dimension is the same as the divergence matrix. The gradient operator, $\mathbf{G}$, takes the parameters

at cell-centers and yields values at cell-faces ($\mathbb{R}^n \rightarrow \mathbb{R}^{n+1}$). The values of ψ and $K(\psi)$ are known on the cell-centers (Figure 3) and must first be averaged to the cell faces; this is completed through harmonic averaging. The ends of the mesh (ψ_1 and ψ_N) are extrapolated to the cell-faces using nearest-neighbour extrapolation.

Figure 3: Cell centered mesh in one-dimension showing a ghost-point

The gradient operator, $\mathbf{G}$, uses a first-order finite-difference approximation. Inhomogeneous Dirichlet boundary conditions are incorporated using a ghost-point outside of the mesh (Figure 3). The value at the boundary face is given by the average $\psi_{\frac{1}{2}} = \frac{1}{2}(\psi_1 + \psi_g)$, which can be put into matrix $\mathbf{G}$ by eliminating ψ_g.

$$\mathbf{G}\psi = \underbrace{\frac{1}{h}\begin{bmatrix} 2 & & & \\ -1 & 1 & & \\ & \ddots & \ddots & \\ & & -1 & 1 \\ & & & -2 \end{bmatrix}}_{\text{Gradient matrix}} \begin{bmatrix} \psi_1 \\ \psi_2 \\ \vdots \\ \psi_{N-1} \\ \psi_N \end{bmatrix} + \underbrace{\frac{1}{h}\begin{bmatrix} -2 & 0 \\ 0 & 0 \\ \vdots & \vdots \\ 0 & 0 \\ 0 & 0 \\ 0 & 2 \end{bmatrix} \begin{bmatrix} \psi_{\frac{1}{2}} \\ \psi_{N+\frac{1}{2}} \end{bmatrix}}_{\text{Inhomogeneous dirichlet boundary condition matrix}} \tag{5}$$

If the boundary conditions are homogeneous Dirichlet ($\psi_{\frac{1}{2}} = \psi_{N+\frac{1}{2}} = 0$) the boundary condition matrix may be dropped. If homogeneous Neumann (no-flux) boundary conditions are needed, the gradient at the boundary face is known to be zero, so this value can be included by a row of zeros in the gradient matrix. The divergence matrix, $\mathbf{D}$ operates from $\mathbb{R}^{n+1} \rightarrow \mathbb{R}^n$ and no boundary conditions are considered. The divergence matrix is a simple first-order difference approximation that yields the values at cell-centers. For a non-regular mesh where $\exists i, j : h_i \neq h_j$ changes in the mesh size must be accounted for in the gradient and divergence matrices. The non-regular mesh has been implemented but will not be discussed in more detail here.

To move to higher dimensions in a tensor-product mesh, Kronecker products may be used to place the finite-difference on the correct cells. For example, the gradient matrix in three-dimensions may be formed by:

$$\begin{aligned} \mathbf{G}_x &= \mathbf{I}_3 \otimes (\mathbf{I}_2 \otimes \mathbf{G}_1) \\ \mathbf{G}_y &= \mathbf{I}_3 \otimes (\mathbf{G}_2 \otimes \mathbf{I}_1) \\ \mathbf{G}_z &= \mathbf{G}_3 \otimes (\mathbf{I}_2 \otimes \mathbf{I}_1) \end{aligned} \tag{6}$$

where $\mathbf{G}_n$ is the gradient operator in one-dimension for the n^{th} dimension. The $\mathbf{I}_n$ is the identity matrix that has the size of the mesh in the n^{th} dimension. Here the full gradient operator can be formed by $\mathbf{G} = [\mathbf{G}_x^\top \quad \mathbf{G}_y^\top \quad \mathbf{G}_z^\top]^\top$. The divergence, and averaging matrices can also be formed using Kronecker products, where $\mathbf{D} = [\mathbf{D}_x \quad \mathbf{D}_y \quad \mathbf{D}_z]$. By focusing on the form of the finite-difference matrices in one-dimension, one can rapidly extend the implementation to simulate two- and three-dimensions.

The gradient and divergence operators are both second-order accurate, due to the staggered mesh implementation. The order of accuracy can be tested on analytic functions where the derivative is known. Testing has been completed in one, two, and three dimensions and shows a decrease of $\mathcal{O}(\delta^2)$ for regular as well as non-regular meshes.

3.2 Time Discretization

Richards equation is often used to simulate water infiltrating into an initially dry soil. At early times in an infiltration experiment the pressure head (ψ) can be close to discontinuous. These large changes in ψ are also reflected in the non-linear terms K and θ; as such, the initial conditions imposed can severely limit the step-size in time if an inappropriate time discretization is chosen. Hydrogeologists are often interested in the process until steady-state is achieve, which may take many time-steps. Considerations of stiffness and length of the time integration point to a numerical scheme that is not limited by stiffness. In this paper I will describe the implementation of a fully-implicit backward Euler

numerical scheme for both the mixed- and head-based formulation (Eq. 1 & Eq. 2). Higher order implicit methods are not considered here because the uncertainty associated with the fitting parameters in the Van Genuchten models (Eq. 3) have much more effect than the order of the numerical method used. The discretized approximation to the mixed-form of Richards equation using fully-implicit backward Euler is:

$$\Phi(\psi^{n+1}, \psi^n) = \frac{\theta(\psi^{n+1}) - \theta(\psi^n)}{\Delta t} - \mathbf{D}\,\mathrm{diag}\left(\frac{1}{\mathbf{A}_v \frac{1}{K(\psi^{n+1})}}\right)\mathbf{G}\psi^{n+1} - \mathbf{D}_z\left(\frac{1}{\mathbf{A}_v \frac{1}{K(\psi^{n+1})}}\right) = 0 \tag{7}$$

To satisfy Richards equation, $\Phi(\psi^{n+1}, \psi^n) = 0$ at the correct ψ^{n+1}. However, because of the nonlinearity it is not possible to directly solve for ψ^{n+1} and an iterative update must be solved for at every time-step. Additionally, the update ψ^{n+1} is contained inside the function for moisture content (θ). To deal with the non-linearity many numerical solutions for Richards equation use the chain rule to separate $\frac{\partial\theta}{\partial t}$ into $\frac{\partial\theta}{\partial\psi}\frac{\partial\psi}{\partial t}$ where $\frac{\partial\theta}{\partial\psi}$ is known from the analytic function in Equation 3.

3.2.1 Head-Based Form

The chain-rule splitting of the time derivative results in the so-called head-based form of Richards equation. Although the splitting of this derivative into components is equivalent in the continuous domain, the discretized version is not and the method may not be conservative [*Celia et al.*, 1990]. However, this method has been historically prevalent in the hydrogeology literature (e.g. *Brunone et al.* [1998]; *Miller et al.* [1998]). Isolating $\frac{\partial\psi}{\partial t}$ allows a Picard iteration ($m = 1, 2, \dots$) to be performed:

$$C(\psi^{n+1,m})\frac{\psi^{n+1,m+1} - \psi^n}{\Delta t} - \mathbf{D}\,\mathrm{diag}\left(K_{Av}^{n+1,m}\right)\mathbf{G}\psi^{n+1,m+1} - \mathbf{D}_z K_{Av}^{n+1,m} = R_P^{n+1,m} \tag{8}$$

where $K_{Av}^{n+1,m} = (\mathbf{A}_v K^{-1}(\psi^{n+1,m}))^{-1}$ and $C(\psi) = \frac{\partial\theta}{\partial\psi}$ and is commonly referred to as the specific moisture capacity function. This equation may be solved for the update to the pressure head $\delta\psi = \psi^{n+1,m+1} - \psi^{n+1,m}$ by rewriting Equation 8.

$$\left(\frac{C(\psi^{n+1,m})}{\Delta t} - \mathbf{D}\,\mathrm{diag}\left(K_{Av}^{n+1,m}\right)\mathbf{G}\right)\delta\psi = \mathbf{D}\,\mathrm{diag}\left(K_{Av}^{n+1,m}\right)\mathbf{G}\psi^{n+1,m} + \mathbf{D}_z K_{Av}^{n+1,m} - C(\psi^{n+1,m})\frac{\psi^{n+1,m} - \psi^n}{\Delta t} \tag{9}$$

The update to the pressure head, $\delta\psi$, can now be found by solving this linear system and updating

$$\psi^{n+1,m+1} = \psi^{n+1,m} + \delta\psi \tag{10}$$

until the residual between inner iterations is sufficiently close to zero. After the Picard iteration is complete ψ^{n+1} is set to the final iterate $\psi^{n+1,m+1}$ and the next time-step can be performed.

3.2.2 Mixed Form - Picard Iteration

The nonconservative nature of the head-based form of Richards equation led *Celia et al.* [1990] to propose the mixed form of the equation. The mixed form does not separate the continuous form of the Richards equation but instead expands using a Taylor series about the m^{th} iterate of θ to approximate $\psi^{n+1,m+1}$.

$$\frac{\theta^{n+1,m+1} - \theta^n}{\Delta t} = \frac{\theta^{n+1,m} + \left.\frac{\partial\theta}{\partial\psi}\right|^{n+1,m}\delta\psi - \theta^n}{\Delta t} + \mathcal{O}(\delta^2) \tag{11}$$

The Taylor series can be linearized and substituted into the mixed form of Richards equation. Rearranging the equation for $\delta\psi$ results in:

$$\left(\frac{C(\psi^{n+1,m})}{\Delta t} - \mathbf{D}\,\mathrm{diag}\left(K_{Av}^{n+1,m}\right)\mathbf{G}\right)\delta\psi = \mathbf{D}\,\mathrm{diag}\left(K_{Av}^{n+1,m}\right)\mathbf{G}\psi^{n+1,m} + \mathbf{D}_z K_{Av}^{n+1,m} - \frac{\theta^{n+1,m} - \theta^n}{\Delta t} \tag{12}$$

This is a very similar to the head-based formulation, and can be solved in a similar way using the Picard iteration and updating $\psi^{n+1,m+1} = \psi^{n+1,m} + \alpha\delta\psi$. The only difference between the head-based form and the mixed-form is in the last term which approximates the time derivative in θ. The mixed-formulation has been shown to be mass conservative *Celia et al.* [1990] and is a superior numerical scheme to the head-based formulation. The Picard iteration, however, may take many iterations to converge and each inner iteration requires solving a linear system of equations. The slow convergence of this fixed-point iteration motivates a more sophisticated root-finding algorithm.

3.2.3 Mixed Form - Newton Iteration

Using a Newton root-finding method can decrease the number of iterations necessary without significantly increasing the size or complexity of the linear system to be solved. The Newton root-finding method iterates over $m = 1, 2, \ldots$ and can be written $\Phi(\psi^{n+1,m}, \psi^n) = R_N^{n+1,m}$ (Eq. 7), where $R_N^{n+1,m}$ is the Newton residual. For Newton root-finding the Jacobian of the system is necessary; the derivative of $\Phi(\psi^{n+1,m}, \psi^n)$ with respect to $\psi^{n+1,m}$ is

$$J_{\psi^{n+1,m}} = \frac{1}{\Delta t}\frac{\partial \theta(\psi^{n+1,m})}{\partial \psi^{n+1,m}} - \frac{\partial}{\partial \psi^{n+1,m}}\left(\mathbf{D}\,\mathrm{diag}\left(K_{Av}^{n+1,m}\right)\mathbf{G}\psi^{n+1,m}\right) - \mathbf{D}_z\frac{\partial K_{Av}^{n+1,m}}{\partial \psi^{n+1,m}} \tag{13a}$$

$$\frac{\partial}{\partial \psi}\left(\mathbf{D}\,\mathrm{diag}\left(K_{Av}\right)\mathbf{G}\psi\right) = \mathbf{D}\,\mathrm{diag}\left(K_{Av}\right)\mathbf{G} + \mathbf{D}\,\mathrm{diag}\left(\mathbf{G}\psi\right)\frac{\partial K_{Av}}{\partial \psi} \tag{13b}$$

$$\frac{\partial K_{Av}}{\partial \psi} = \mathrm{diag}\left((\mathbf{A}_v K^{-1}(\psi))^{-2}\right)\mathbf{A}_v\,\mathrm{diag}\left(K^{-2}(\psi)\right)\frac{\partial K(\psi)}{\partial \psi} \tag{13c}$$

Here the analytical derivatives of the Van Genuchten equations are needed. It should be noted that when ψ is a vector these derivatives are diagonal matrices.

$$C(\psi) = \frac{\partial \theta}{\partial \psi} = -\frac{\alpha(\theta_s - \theta_r)}{(\alpha + |\psi|^\beta)^2}\beta|\psi|^{\beta-1}\mathrm{sign}(\psi) \tag{14a}$$

$$\frac{\partial K}{\partial \psi} = -K_s\frac{A}{(A + |\psi|^\gamma)^2}\gamma|\psi|^{\gamma-1}\mathrm{sign}(\psi) \tag{14b}$$

To have a fully inplicit scheme, the update to $n+1$ requires a non-linear solve. This is completed by using a Newton root finding technique.

$$\Phi(\psi^{n+1,m} + \delta\psi, \psi^n) = \Phi(\psi^{n+1,m}, \psi^n) + J_{\psi^{n+1,m}}\delta\psi + \mathcal{O}(\delta^2) \tag{15}$$

so the update $\partial\psi$ can be found by linearizing, setting Equation 15 to zero, and solving the linear system

$$\delta\psi = -J_{\psi^{n+1,m}}^{-1}\Phi(\psi^{n+1,m}, \psi^n) \tag{16}$$

The iteration is completed by adding the Newton update to the last iterate

$$\psi^{n+1,m+1} = \psi^{n+1,m} + \alpha\delta\psi \tag{17}$$

The pure Newton step may also overshoot the root; to prevent this, a simple back-tracking linesearch is used to ensure a sufficient decrease in $R_N^{n+1,m}$. The Newton root-finding method must solve a linear system of an equal size to the Picard iteration. However, when the initial guess is close to the actual solution (i.e. ψ^n is close to ψ^{n+1}) the Newton method converges quadratically, reducing the number of times the linear system must be solved. It is noted that the Jacobian may have negative eigenvalues, which will cause the root-finding algorithm to diverge. The implementation often fails when the boundary conditions are not honored in the initial conditions or the conditions in the soil column are discontinuous and changing rapidly. If the Newton iteration fails to converge to a solution the update is performed with the less efficient but equivalent mixed-form Picard iteration discussed above.

4 Code Testing - Ficticious Source

Richards equation has no analytic solution, which makes testing of the code more involved. We use a fictitious source experiment to rigorously test the code. In this experiment we will approximate an infiltration front by an arctangent function centered over the highly nonlinear part of the Van Genuchten curves in Figure 1. The arctangent curve advects into the soil column with time. The advantage of using an analytic function is that the derivative is known explicitly and can be calculated at all times. However, it should be noted that Richards equation does not satisfy the analytic solution exactly, but differs by a function $S(x,t)$; this function is referred to as the fictitious source term. The analytic function used has similar boundary conditions and shape to the previous example, and is considered over the domain $x \in [0,1]$.

$$\Psi_{\text{true}}(x,t) = -20\arctan(20((x - 0.25) - t)) - 40 \tag{18}$$

This analytic function is shown at time 0 and time 0.5 in Figure 4 and has a pressure head range of $\psi \in [-60, -20]$; these values can be directly compared to the Van Genuchten curves in Figure 1. The known pressure head can then be

put directly into Richards equation (Eq. 1) and the analytic derivatives can be calculated and equated to a source term $S(x,t)$. Knowing this source term and the analytic boundary conditions the discretized form of Richards equation can be solved, and should reproduce the analytic function in Equation 18. Table 1 shows the results of the fictitious source test when the number of mesh-cells is doubled; the time-discretization is fixed and is the same as the mesh size (i.e. $k = h$). In this case it is expected that the order of accuracy should be limited by the backward-Euler time discretization, which is $\mathcal{O}(\delta)$. The final column of Table 1 indeed shows that the order of accuracy is $\mathcal{O}(\delta)$. The higher errors in the coarse discretization is due to the high discontinuities and changes in the source term, which the coarse discretizations do not resolve. A similar procedure can be completed in two and three dimensions, and these tests also show the same results. The rigorous testing of the code presented provides confidence in the results that are described in the following sections of this paper.

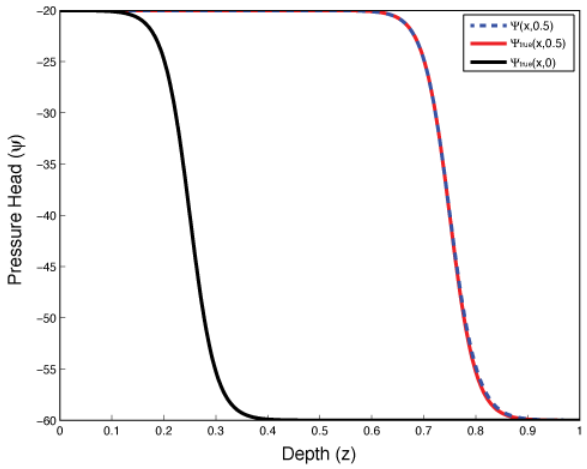

Figure 4: Ficticious source test in 1D showing the analytic function Ψ_{true} at times 0.0 and 0.5 and the numerical solution $\Psi(x, 0.5)$ using the mixed-form Newton iteration

Table 1: Ficticious Source Test in 1D using the mixed-form Newton iteration

Mesh Size (n)	$\|\|\Psi(x,0.5) - \Psi_{\text{true}}(x,0.5)\|\|_\infty$	Order Decrease
64	5.485569e+00	
128	2.952912e+00	0.894
256	1.556827e+00	0.924
512	8.035072e-01	0.954
1024	4.086729e-01	0.975
2048	2.060448e-01	0.988
4096	1.034566e-01	0.994
8192	5.184507e-02	0.997

5 Results

The first results presented here are a direct comparison to the results produced by *Celia et al.* [1990] for the Picard iteration only, *Celia et al.* [1990] did not implement the Newton iteration. The direct comparison is completed (a) to give confidence to the numerical results; and (b) to compare the Newton iteration to the Picard iteration of the mixed formulation for a well known example. The parameters for the Van Genuchten equations (Eq. 3) are again the ones shown in Figure 1 and are $\alpha = 1.611 \times 10^6$, $\theta_s = 0.287$, $\theta_r = 0.075$, $\beta = 3.96$, $A = 1.175 \times 10^6$, $\gamma = 4.74$, $K_s = 9.44 \times 10^{-5}$ m/s [*Celia et al.*, 1990]. The initial conditions of a 40cm high 1D soil column are initially dry

with a pressure head $\psi_0(x, 0) = -61.5$cm. The boundary conditions applied are inhomogeneous Dirichlet with the top of the soil column $\psi(40\text{cm}, t) = -20.7$cm, and the bottom of the soil column $\psi(0\text{cm}, t) = -61.5$cm. The initial conditions are not consistent with the boundary condition at the top of the soil profile. This inconsistency leads to a boundary layer and a steep gradient in the pressure head at early times, as such, it is anticipated that the Newton iteration will not converge at early times. The spatial grid is regular and has a spacing of 1cm, while the time stepping, Δt, is manipulated. The three iterative methods described in Section 3.2 are implemented and compared at 360s: (1) head-based form Picard; (2) mixed-form Picard; and (3) mixed-form Newton. The solution obtained with the three iterative methods is shown in Figure 5. Comparing the head-based formulation to the mixed-formulation for a large time-step (e.g. $\Delta t = 120$s) shows the degradation of the head-based method. Not only is the infiltration front smoothed, there is severe underestimate of the front location (Figure 5(a)). The underestimate of the infiltration front location is due to a loss of mass, which can be traced back the initial formulation of the head-based method [*Celia et al.*, 1990]. The mixed-formulation, solved with either a Picard iteration or a Newton method, conserves mass and correctly identifies the spatial location of the infiltration front (Figure 5(b)). Comparing the results obtained here to *Celia et al.* [1990] shows excellent agreement.

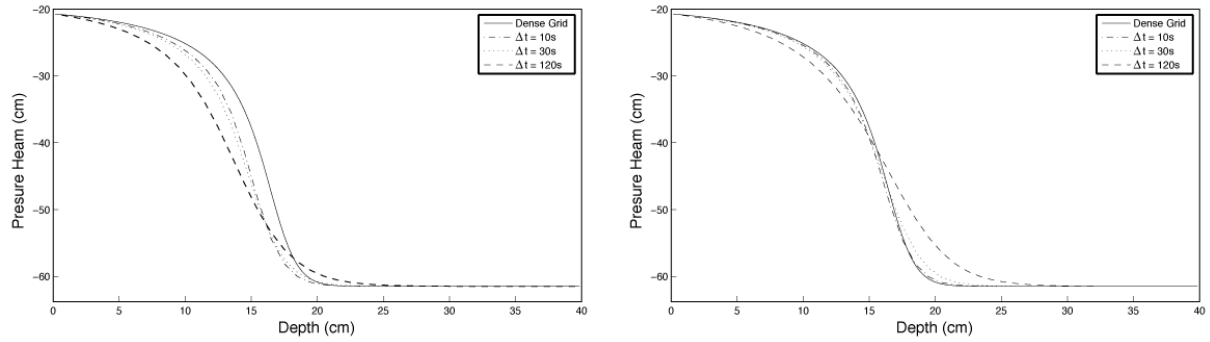

(a) Head-based formulation (Picard Iteration)

(b) Mixed formulation (Picard/Newton Iteration)

Figure 5: Comparison of results to *Celia et al.* [1990] showing the differences in the head-based and mixed formulations at t=360s.

5.1 Comparison of Iterative Methods

With the goal of extending these simple one-dimensional examples into three-dimensions, the efficiency of the iterative method used is of critical importance for computational solve time. A comparison of the iterative methods used for the numerical example described above (where $\Delta t = 10$s) is seen in Figure 6. It is seen that both of the Picard schemes take between 10 and 25 iterations per time-step, while the Newton scheme generally uses less than five iterations (Figure 6(a)). The difference between iteration counts is due to the use of the gradient information in the Newton method, which speeds convergence when the initial guess is close to the solution. When the initial guess is not close, for example at $t = 0$s, the Newton method fails to converge and a Picard iteration is used. The first iteration of Newton is higher in both the number of iterations and solve time (Figure 6(b)). In both Figure 6(a) & 6(b) there is a overall decrease in the number of iterations used. As the system reaches steady-state the number of iterations required to move between time-steps is reduced. The overall results of solve time and total iterations is seen in Table 2. The Newton method is marginally faster than either of the Picard iterations as Newton takes the fewest number of iterations. As the size of the problem increases and moves to higher dimensions the number of iterations increases slightly, however, the time to solve the systems dramatically increases. The Newton method has clear advantages when moving to larger two- and three-dimensional models.

Table 2: Comparison of total solve time and iteration of numerical schemes ($\Delta t = 10$s)

Method Name	Solve Time (s)	Total Iterations
Head-Picard	1.721	501
Mixed-Picard	1.574	479
Mixed-Newton	1.381	112

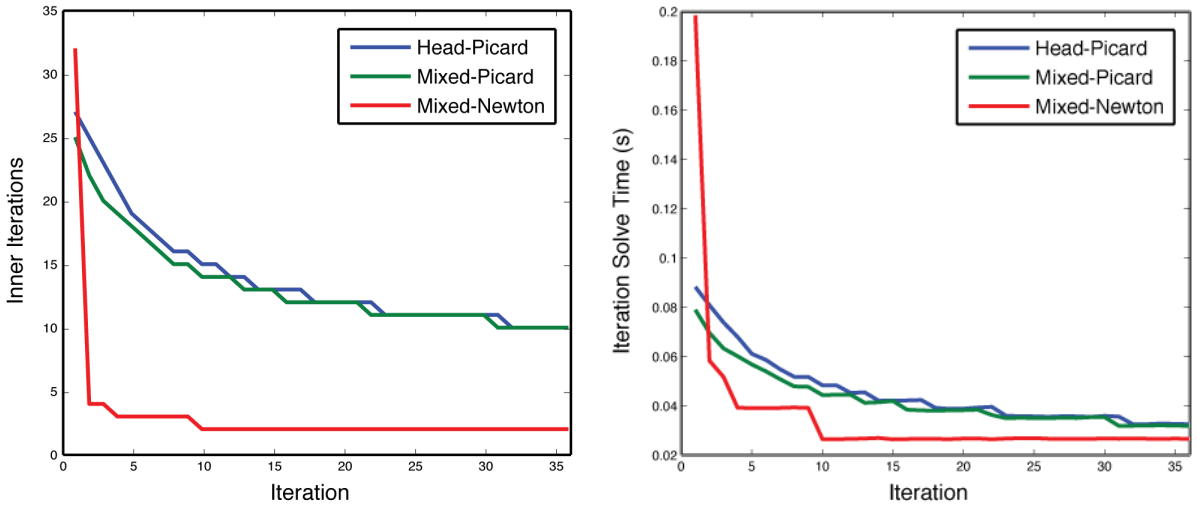

(a) Number of inner iterations per iteration

(b) Solve time per iteration

Figure 6: Comparison of iterative schemes ($\Delta t = 10$s)

5.2 Example in two-dimensions

Infiltration into a heterogeneous porous media is a common problem in hydrogeology. Here a simplified two-dimensional media is presented that simulates a discontinuous silt layer, which has a lower hydraulic conductivity. The outline of the silt layer is shown with thick black rectangles in Figure 7. The background has a hydraulic conductivity of 1×10^{-2} m/s (sand), the discontinuous silt layer has a hydraulic conductivity of 5×10^{-3} m/s. The initial saturation of the system is set to 10% ($\psi = -60$cm). Neumann (no-flow) boundary conditions are applied to all boundaries of the model. To simulate an infiltration experiment a source term of 150mL/min is added to the top row of the model. The amount of water added to the system will eventually saturate the media, however, the distribution of water over the first few hours is of interest. The model was discretized with a 1cm grid in both horizontal and vertical directions, the time step was chosen to be 10s. The choice of time-step was based on the comparisons in Figure 5; $\Delta t = 10$s provides an accurate simulation of the infiltration front. For simplicity, the Van Genuchten parameters used are the same as the previous two examples.

The expected results are downward flow that is faster in the sand than in the silt. Additionally, at late times it is expected that there should be an accumulation of water on the top of the silt layer because of the semi-impermeable barrier. The results for two time-steps are shown in Figure 7. The saturation contours are farther apart in the sand indicating a faster movement of water in the more conductive material. At both time steps the saturation contours refract into the lower conductivity silt layer and there are large changes in saturation between the top and bottom of the silt. In Figure 7(b) when the water has been flowing for 3.06 hours some ponding of water has occurred above the silt layer. This numerical example shows the extensible nature of the code developed to simulate heterogeneous systems in many dimensions.

6 Discussion & Conclusions

In this paper I have shown a fully-implicit backward Euler discretization of Richards equation. The non-linearity present in the equation has been dealt with by using a Newton-root finding algorithm. The work here has excellent correspondence to results produced by a seminal paper in the literature that used a Picard iteration to deal with the nonlinearity [*Celia et al.*, 1990]. The Newton root-finding scheme implemented here was found to take fewer iterations than the equivalent Picard iteration, and was on average faster. The speed for evaluating Richards equation is important when framing the inverse problem: 'Given the saturation distribution over time, what is the hydraulic conductivity?' The inverse framework requires many simulations of Richards equation and computational time is often a bottleneck of the problem.

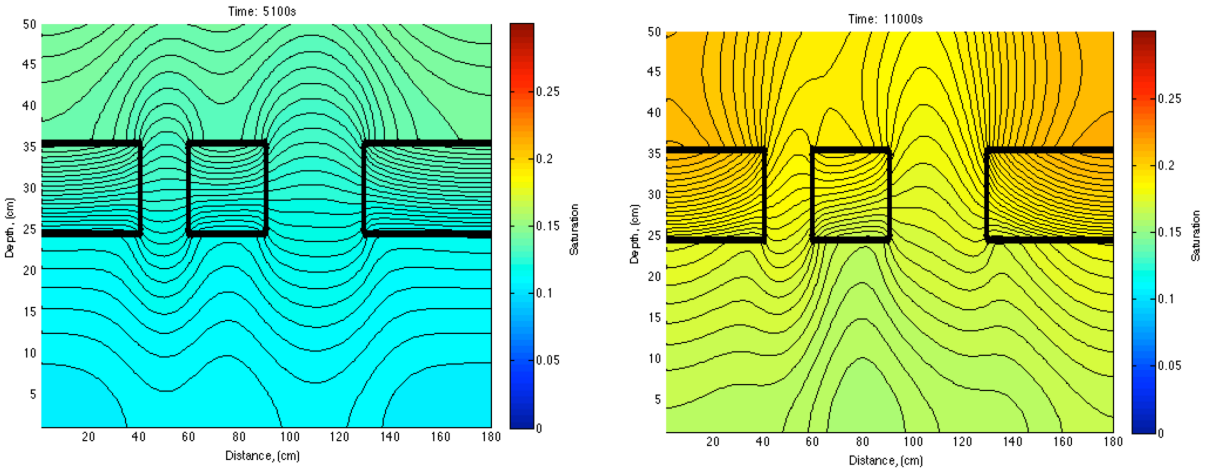

(a) Time: 5100s (1.42 hrs)

(b) Time: 11000s (3.06 hrs)

Figure 7: Simulation of a discontinuous clay layer (outlined in black) showing saturation profiles at two time-steps.

The work completed here is a first step at tackling the inverse problem, and requires minor adjustments to improve speed and reliability. Referring to the decreased number of iterations over time (Figure 6) suggests that larger time steps may be taken and a variable time-stepping scheme should be implemented. Additional numerical checks, such as mass-balance evaluation should also be implemented. The work presented has been heavily tested, both with the fictitious source test, direct comparisons to the literature, and every analytic derivative and numerical operator. The results of the numerical tests, are attached as an appendix. The focus on the robustness of the code, through the use of testing each component, lends validity to the interpreted results when using this code in practice.

Acknowledgments

I would like to thank Eldad Haber for his useful insight into the different formulations and methods developed in this paper. I would also like to thak Uri Ascher for a excellent introduction into numerical methods for differential equations.

References

Brunone, B., M. Ferrante, N. Romano, and A. Santini, Numerical Simulations of One-Dimensional Infiltration into Layered Soils with the Richards Equation Using Different Estimates of the Interlayer Conductivity, pp. 193–200, 1998.

Celia, M. A., E. T. Bouloutas, and R. L. Zarba, A general mass-conservative numerical solution for the unsaturated flow equation, *Water Resources Research*, *26*(7), 1483–1496, doi:10.1029/WR026i007p01483, 1990.

Miller, C. T., G. a. Williams, C. T. Kelley, and M. D. Tocci, Robust solution of Richards' equation for nonuniform porous media, *Water Resources Research*, *34*(10), 2599, doi:10.1029/98WR01673, 1998.

van Genuchten, M. T., A Closed-form Equation for Predicting the Hydraulic Conductivity of Unsaturated Soils, *Soil Science Society of America Journal*, *44*(5), 892, doi:10.2136/sssaj1980.03615995004400050002x, 1980.